

The Aethalometer calibration and determination of iron concentration in dust aerosols

P. Fialho^{a,*}, M.C. Freitas^b, F. Barata^a, B. Vieira^b, A.D.A. Hansen^c, R.E. Honrath^d

^a*Grupo de Química e Física da Atmosfera, Universidade dos Açores, PT-9701-851 Terra Chã, Portugal*

^b*Instituto Tecnológico e Nuclear-Reactor, Apartado 21, EN10 Sacavém, PT-2685-953 Sacavém, Portugal*

^c*Lawrence Berkeley National Laboratory, Berkeley, CA 94720, USA*

^d*Department of Civil & Environmental Engineering, Michigan Technological University, Houghton, MI 49931, USA*

Received 13 October 2005; received in revised form 9 February 2006; accepted 5 March 2006

Abstract

This paper shows the use of the instrumental neutron activation analysis (INAA) technique to calibrate Aethalometer instruments' response to iron oxides present in Saharan dust aerosol. The five samples selected for this calibration were collected with a seven-wavelength Aethalometer (model AE31) at the summit of Pico mountain (2225 m ASL) in the Azores Islands. These samples correspond to measurements taken between the 31 October and 5 November, 2001. Analysis of these samples by the INAA technique gave a total mass of $14.84 \pm 0.70 \mu\text{g (Fe)}$. Correlation of the analytical results with the optical measurements allowed the determination of the elemental iron calibration constant, K_{Fe} ($0.234 \pm 0.022 \mu\text{m}^4 \text{m}^2 \text{g}^{-1}$), which can be used in the determination of iron concentrations from multi-wavelength Aethalometer measurements. As an example of this, we used Aethalometer measurements during the 2001 event to calculate hourly average dust iron, $\langle C_{\text{Fe}} \rangle$, concentrations, which range from 0.00 and $1.77 \mu\text{g (Fe) m}^{-3}$.
© 2006 Elsevier Ltd. All rights reserved.

Keywords: Aethalometer calibration; Absorption coefficient; Black carbon; Sahara dust; PICO-NARE; Seven-wavelength aethalometer; INAA technique; Hematite; Iron oxides

1. Introduction

The PICO-NARE observatory is an experimental site on the summit of the Pico Mountain (38.470°N ; 28.404°W ; 2225 m altitude) in the Azores archipelago (Honrath & Fialho, 2002; Honrath et al., 2004). This site is in the pathway of air masses travelling from surrounding continents (Africa, Europe and Central and North America) that carry with them, among other species, aerosols resulting from anthropogenic and natural emissions.

In particular, transport of combustion emissions from North America or Europe may bring black carbon particles to the Azores region, while transport from Africa may bring soil dust particles (Fialho, Hansen, & Honrath, 2005). Black carbon (BC) aerosols are an important atmospheric component because of their potential deleterious impact on health and climate (Baumgardner et al., 2002), and dust, resulting from natural emissions, is involved in the biogeochemical cycling of iron, an essential micronutrient for marine phytoplankton (Arimoto, Balsam, & Schloesslin, 2002). Both BC (Bohren & Huffman, 1998; Lindberg, Douglass, & Garvey, 1993; Ackerman & Toon, 1981; Bodhaine, 1995) and dust

* Corresponding author. Tel.: +351 295 402 237; fax: +351 295 402 205.

E-mail address: paulo.fialho@mail.angra.uac.pt (P. Fialho).

(Gillespie & Lindberg, 1992; Caquineau, Gaudichet, Gomes, Magonthier, & Chatenet, 1998) particles absorb light at visible wavelengths, and therefore both, if present, contribute to measurements of the aerosol absorption coefficient, $\sigma_{\text{aerosol}}(\lambda, t)$, of the type reported here. Previously, we proposed a method to separate these two contributions (Fialho et al., 2005), based on the linear combination of two types of aerosol absorption coefficient to the measured absorption coefficient,

$$\sigma_{\text{aerosol}}(\lambda, t) = \sigma_{\text{BC}}(\lambda, t) + \sigma_{\text{dust}}(\lambda, t), \quad (1)$$

where $\sigma_{\text{BC}}(\sigma, t)$ and $\sigma_{\text{dust}}(\sigma, t)$ are, respectively, the BC and dust absorption coefficients.

We focus our attention here on the iron concentrations results, because iron is a tracer for the iron oxides present in Saharan dust aerosol. Five spots of aerosol (codes SPOT111 through SPOT115) were selected according to their reddish brown colour. This colouration is associated with mineral dust (Tomza, Arimoto, & Ray, 2001; Sokolik & Toon, 1999) rich in a mixture of iron oxide with predominance of iron (III) (Fe_2O_3), also known as hematite (Arimoto et al., 2002, mindat.org). These sample spots were analyzed for elemental content by using the instrumental neutron activation analysis technique (INAA) at the ITN (Technological and Nuclear Institute of Portugal) laboratories. This technique was previously described by several authors (Freitas & Martinho, 1989; Alves, Reis, & Freitas, 1998a, 1998b; Farinha, Freitas, Almeida, & Reis, 2001; Freitas, Almeida, Reis, & Oliveira, 2003).

This instrumentation is used to calibrate the Aethalometer measures, allowing the determination of the time varying iron concentrations associated with the mineral dust. This information will allow improving the lack of quantitative information available related to the mineral dust impacts on the radiative forcing (Coen et al., 2003; Sokolik & Toon, 1999).

2. Experimental setup and uncertainties

In this and the following section, when values are presented with uncertainties in the form $x \pm dx$ (where x is the value and dx the corresponding uncertainty), the stated uncertainties have the following meaning. For values obtained directly from the raw measurements, the experimental uncertainty (95% confidence interval) is used. For values calculated from the raw measurements, the uncertainties in the underlying measurements are propagated. For values obtained from regression analyses, the standard deviation of the parameter is used.

2.1. Characterization of sampled aerosol

The selected period, from 17:15 UTC 31 October till 16:30 UTC 5 November, 2001, corresponds to the largest detected dust event in the Azores archipelago during 2001 with origin in Africa. For this period we classified the measurements according to the PICO-NARE observatory environmental conditions, if it was in free troposphere (FT) or under the influence of the marine boundary layer (MBL).

High values of relative humidity ($\text{RH} > 90\%$) can be associated with the PICO-NARE station being in the MBL. However, RH alone is not a reliable indicator of upslope flow of MBL air. We analyzed the temperature inversion heights during the study period to determine the MBL or FT conditions of the site. The temperature inversion height was taken from the vertical profile of the temperature data available from the FSL/NCDC Radiosonde Data Archive (FXL/NCDC) for station ID:08508 (Lajes - Terceira). The radiosonde data analyses show that from the 11h UTC, 1 November, 2001 till 11h UTC, 4 November, 2001 the MBL was significantly below (less than 2000 m) the height of the observatory station (2225 m). For the remaining portion of the event discussed here, the temperature inversion was very near the site height or even above it. These Radiosondes are launched at a distance of about 120 km from the PICO-NARE site. As a result of the orographic effect, due to the presence of the mountain, upslope flow of the MBL air mass around the mountain can occur and impact the PICO-NARE site. As a result, and taking in consideration the high values of the relative humidity ($> 90\%$), the period before 7:30 UTC 1 November, 2001, and after 4:30 UTC 4 November, 2001, was considered to be influenced by the MBL. In between these times, the site is presumed to be under FT conditions (Fig. 1). This approach is in agreement with the estimates obtained by using the Sheppard's airflow model (Kleissl & Honrath, 2005), which take in consideration orographic lifting and the occurrence of mountain clouds. That model, applied by Kleissl (2005) to the period under study uses as input the FNL data. Results were obtained with a 6 hour resolution interval and suggest that between 12h UTC 30, October and 12h UTC 4, November, 2001 the site was exposed to FT air.

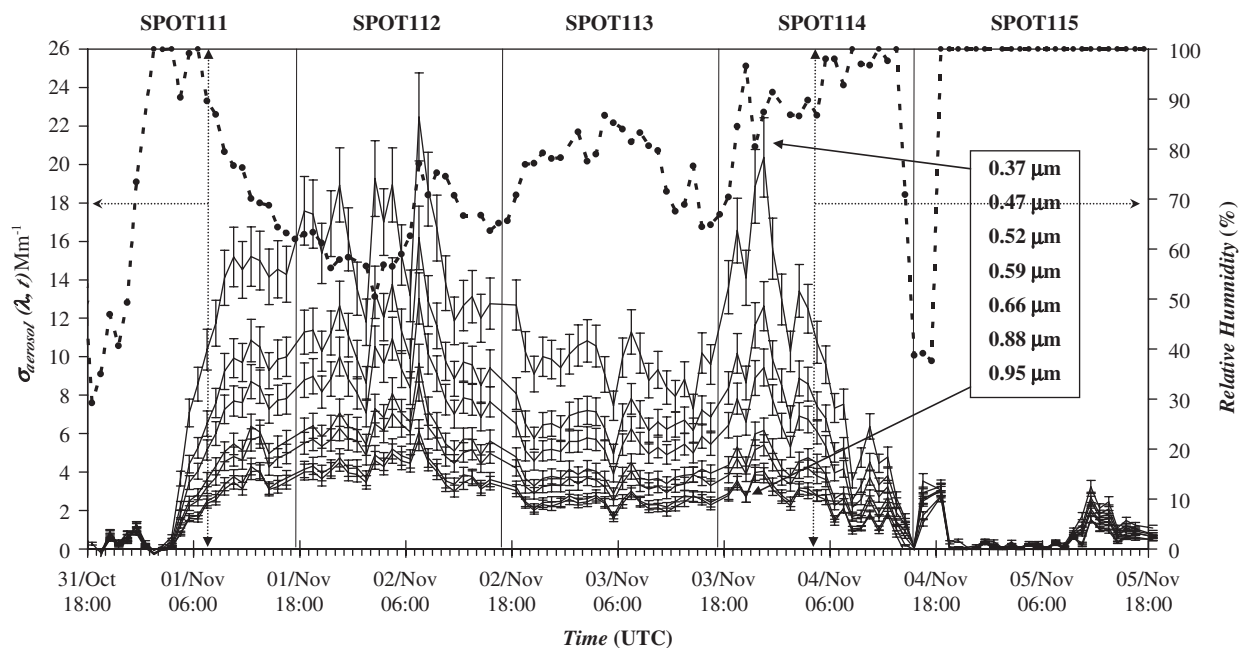


Fig. 1. Solid lines with error bars, represent aerosol absorption coefficients levels calculated from applying Eqs. (2) and (3) to the measured Aethalometer information, obtained at the PICO-NARE observatory, during the period from the late afternoon of October 31 through midday November 5, 2001. Aerosol absorption coefficients are inversely proportional to the wavelength (see legend with only the extreme wavelengths associated to the lines with the arrows). Dashed lines with dots, represent the relative humidity at the sample site during the measurement. Vertical solid lines are used to separate the data associated with each of the filter spots (each of which is referenced by a label, e.g., Spot111). Vertical dashed lines, with horizontal dashed arrow, isolate the periods classified as corresponding to the MBL (extremes) and FT (in between).

To characterize the transport pathways and potential aerosol source regions associated with the aerosol sampled during the period under study, 5-day synoptic backward trajectories were calculated. The hybrid single-particle lagrangian integrated trajectories (HYSPLIT) model, (Draxler & Rolph, 2003; Draxler & Hess, 1997, 1998) was used with meteorological data from the National Weather Service's National Center for Environmental Prediction (NCEP) FNL data set (Stunder, 1997). The data are available every 4 h on a 129 by 129 point hemispheric stereographic grid with output on 13 mandatory pressure levels and the surface level. Backward trajectories were calculated every hour. At these times, a set of 27 trajectories was initiated. Three sets of nine end point trajectories at heights 2125 m, 2225 m and 2325 m were made, with each set having one trajectory terminating at the PICO-NARE observatory coordinates, and eight terminating at end points separated by 1° of latitude and longitude from the observatory coordinates.

Hourly analyses of the backward trajectories (HYSPLIT) showed that, during the full duration of the event under study, the sampled air could be associated with upwind transport over Africa. During short portions of the event, the trajectories indicate the potential for European and/or North American influence as well. However, the presence of African dust aerosol is supported by analysis of daily averaged aerosol optical depth (AOD) from the MODIS satellite (Hubanks, Remer, & Kaufman (MODIS)). By correlating the back trajectory simulation trajectories with the AOD satellite images, we verify that the back trajectories crossed regions of enhanced AOD due to the presence of aerosol, whose source is associated with the African continent.

2.2. The Aethalometer

The Aethalometer system used here was previously described by Fialho et al. (2005). Aethalometer measurements of aerosol absorption coefficients have been made at the PICO-NARE observatory since July 2001.

The period under study corresponds to five filter spot samples with area, A , of $0.50 \pm 0.05 \text{ cm}^2$, started at 17:15 UTC on 31 October, 2001, and ending at 16:30 UTC on 5 November, 2001. SPOT112 corresponds to an aerosol accumulation period of $22.7500 \pm 0.0048 \text{ h}$ and the other four spots to accumulation periods of $23.6667 \pm 0.0048 \text{ h}$.

During all these periods, intensity values ($I_S(\lambda, t)$ and $I_R(\lambda, t)$ are, respectively, the intensities measured after the beam crossed the sample and reference filter spot areas) at seven wavelengths (0.37, 0.47, 0.52, 0.59, 0.66, 0.88 and 0.95 μm) were measured at 5 min intervals. The average flow rate, $\langle F(t) \rangle$, in units of standard litre per minute (SLPM), was measured with one internal mass flowmeter (Sierra Model 824); the sample flow was provided by a diaphragm external vacuum pump (KNF Neuberger, Model UN85.3). The quartz fibre filter tapes are manufactured by Pallflex[®] (type: Q250F). Aerosol absorption coefficients, $\sigma_{\text{aerosol}}(\lambda, t)$, were calculated for a differentiation interval (Δt) corresponding to the spots accumulation time or one hour period, and referred to the appropriated interval centered time ($t_0 + \Delta t/2$). The theoretical grounds for the Aethalometer measurements and respective errors were previously reported by Fialho et al. (2005),

$$\sigma_{\text{aerosol}}(\lambda, t) = \frac{A}{\langle F(t) \rangle} \times \frac{\text{ATN}(\lambda, t) - \text{ATN}(\lambda, t_0)}{\Delta t}, \quad (2)$$

where the attenuation values, $\text{ATN}(\lambda, t)$, values are calculated from the intensity values according to the expression,

$$\text{ATN}(\lambda, t) = -\ln \left(\frac{I_S(\lambda, t)}{I_R(\lambda, t)} \right). \quad (3)$$

The 1 h calculated absorption coefficients, $\sigma_{\text{aerosol}}(\lambda, t)$, for the period in study, ranged from 0.0 to 22.5 Mm^{-1} (Fig. 1), with standard deviations lower than a maximum of 2.3 Mm^{-1} . The results of application of Eqs. (2) and (3) to the experimental values measured at the time corresponding to the beginning (t_0) and end (t) of the sample spot are presented in Table 1. (Δt for each spot can be seen in the same table).

2.3. The instrumental neutron activation analysis (INAA)

The collected quartz filter spots (SPOT111 through SPOT114) showed a reddish brown coloration while the SPOT115 is so light that it was very difficult to see any coloration at all. These spots were identified after removing the tape from the Aethalometer in early July, 2002, and were packed together with unexposed portions of the tape (as blanks) and analyzed for elemental composition at ITN (Instituto Tecnológico e Nuclear).

At ITN the blanks and the sampled filters were cut from the strips in circular forms with area $0.950 \pm 0.086 \text{ cm}^2$. These circular cutouts were centered on the sampled area ($0.50 \pm 0.05 \text{ cm}^2$). The exposed side of each spot was covered with piece of the unexposed blank filter, to avoid contamination of the sample with the polyethylene top cover; the same procedure was applied to each blank in order to obtain identical geometry. Each sandwiched set was weighed in a 0.1 μg sensitivity balance and packed into aluminum sheets.

Each sample or blank sandwiched set was irradiated for 11 h with a thermal flux of $1.124 \times 10^{13} \text{ cm}^{-2} \text{ s}^{-1}$ together with one disc (125 μm thick and 0.5 cm of diameter) of a 0.1% Au–Al alloy as comparator. After irradiation, samples decayed for 4 to 6 days and were then measured; after this measurement samples decayed for 2 to 3 weeks more and were measured again. The gamma spectra measurements for each sample were collected on a liquid nitrogen-cooled, ORTEC calibrated hyperpure germanium detector (1.85 keV resolution at 1.33 MeV and 30% relative efficiency), connected to a 4096 multi-channel analyzer. The gold alloy disk was also measured with the same detector 7 days after the end of the irradiation. The determination of the elemental composition of iron resulted from the application of the k_0 -standardization method described by De Corte (1987).

The estimated iron mass and concentration obtained for each of the five sampled spots, after correction for blank levels ($0.48 \pm 0.12 \mu\text{g}$), are presented in Table 2.

3. Results and discussion

Considering the approach of Fialho et al. (2005) to decouple the contribution of BC and dust from the aerosol absorption coefficient given by

$$\sigma_{\text{aerosol}}(\lambda, t) \times \lambda^{-\alpha} = K_{\text{BC}} \langle C_{\text{BC}}(t) \rangle + K_{\text{dust}} \langle C_{\text{dust}}(t) \rangle \lambda^{\beta-\alpha}, \quad (4)$$

where K_{BC} and K_{dust} are, respectively, black carbon and dust empirical constants that should be obtained from calibration of the instrument, and $\langle C_{\text{BC}}(t) \rangle$ and $\langle C_{\text{dust}}(t) \rangle$ are the average concentrations of black carbon and dust, respectively. For the corresponding

Table 1

Aerosol absorption coefficients, $\sigma_{\text{aerosol}}(\lambda, t)$, estimated from the application of Eqs. (2) and (3) to the five spots time intervals, Δt , for each one of the seven wavelengths (λ 's are 0.37, 0.47, 0.52, 0.59, 0.66, 0.88 and 0.95 in μm)

Sample	$\sigma_{\text{aerosol}}(0.37, t)$ (Mm^{-1})	$\sigma_{\text{aerosol}}(0.47, t)$ (Mm^{-1})	$\sigma_{\text{aerosol}}(0.52, t)$ (Mm^{-1})	$\sigma_{\text{aerosol}}(0.59, t)$ (Mm^{-1})	$\sigma_{\text{aerosol}}(0.66, t)$ (Mm^{-1})	$\sigma_{\text{aerosol}}(0.88, t)$ (Mm^{-1})	$\sigma_{\text{aerosol}}(0.95, t)$ (Mm^{-1})	$\langle F(t) \rangle \times 10^3$ ($\text{m}^3 \text{min}^{-1}$)	Δt (min)
SPOT111	7.00 ± 0.72	4.67 ± 0.48	3.70 ± 0.38	2.64 ± 0.27	2.36 ± 0.24	1.75 ± 0.18	1.67 ± 0.17	3.421 ± 0.081	1420.00 ± 0.29
SPOT112	15.6 ± 1.6	11.0 ± 1.1	8.83 ± 0.90	6.43 ± 0.65	5.74 ± 0.58	4.28 ± 0.43	4.03 ± 0.41	3.313 ± 0.055	1365.00 ± 0.29
SPOT113	9.8 ± 1.0	6.78 ± 0.70	5.42 ± 0.56	3.90 ± 0.40	3.45 ± 0.36	2.57 ± 0.27	2.42 ± 0.25	3.435 ± 0.077	1420.00 ± 0.29
SPOT114	9.33 ± 0.96	6.13 ± 0.63	4.77 ± 0.49	3.35 ± 0.34	2.97 ± 0.30	2.22 ± 0.23	2.09 ± 0.21	3.451 ± 0.080	1420.00 ± 0.29
SPOT115	0.881 ± 0.090	0.697 ± 0.071	0.623 ± 0.064	0.489 ± 0.050	0.467 ± 0.048	0.341 ± 0.035	0.377 ± 0.038	3.461 ± 0.066	1420.00 ± 0.29

Respective average flux, $\langle F(t) \rangle$, during the sample period, Δt , are also shown. Each value is shown with the respective standard error.

Table 2

Iron mass, m_{Fe} , estimated for each spot analyzed by the INAA technique

Sample	$V (\text{m}^3)$	$m_{\text{Fe}} (\mu\text{g})$	$\langle C_{\text{Fe}}(t) \rangle (\mu\text{g m}^{-3})$
SPOT111	4.86 ± 0.12	2.23 ± 0.36	0.459 ± 0.074
SPOT112	4.522 ± 0.075	5.19 ± 0.36	1.148 ± 0.083
SPOT113	4.88 ± 0.11	3.68 ± 0.33	0.754 ± 0.070
SPOT114	4.90 ± 0.11	3.04 ± 0.30	0.620 ± 0.064
SPOT115	4.915 ± 0.094	0.70 ± 0.18	0.142 ± 0.036

Volume, V , of air sampled during the period of the spot mass accumulation and the average iron mass concentration, $\langle C_{\text{Fe}}(t) \rangle$, estimated during the sample period of each spot. Each value is shown with the respective standard error.

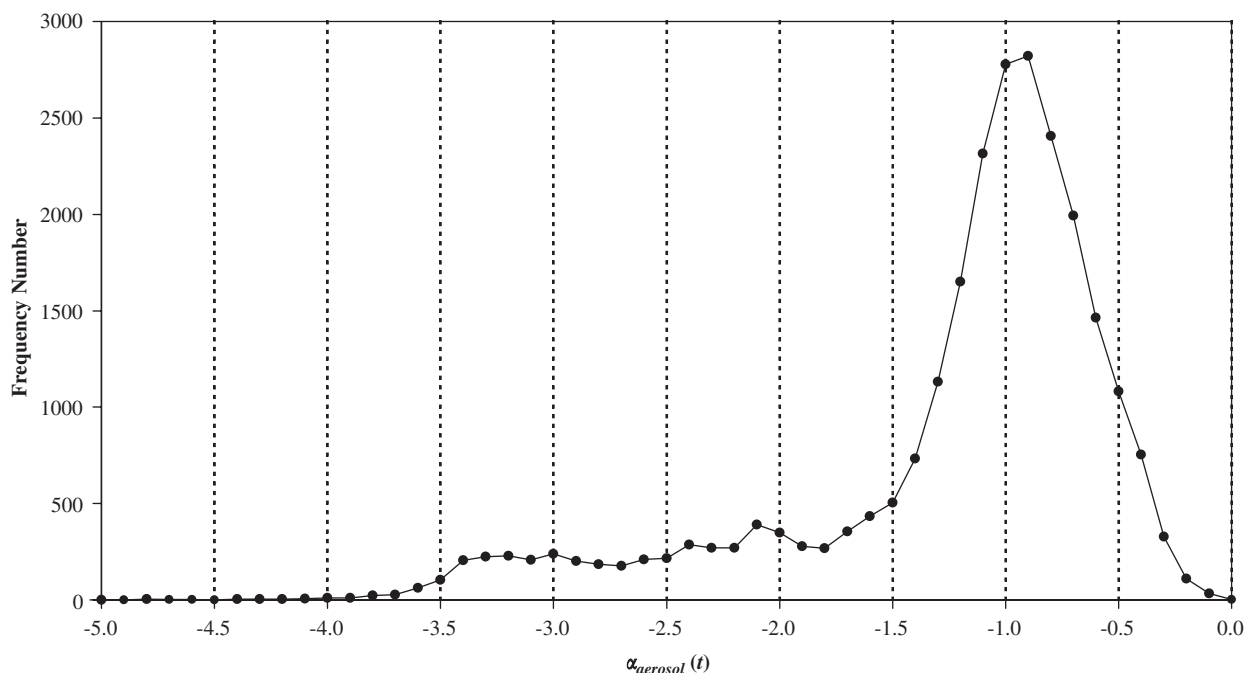


Fig. 2. Solid line with solid circles represent the frequency number of the $\alpha_{\text{aerosol}}(t)$, estimated from applying Eq. (5) to all the hourly available measurements of aerosol absorption coefficients made at the PICO-NARE site during July, 2001 through June 2005.

time period (t), α and β are, respectively, the BC and dust absorption exponents that translate the wavelength dependence of the absorption coefficient due to the presence of BC and dust. The values of α and β were determined from the histogram plot shown in Fig. 2. To elaborate this histogram we used the approach described by Fialho et al. (2005), where the empirical working equation of the Aethalometer given by Eq. (17) (Fialho et al., 2005) is transformed in a linear form at each time, t ,

$$\ln[\sigma_{\text{aerosol}}(\lambda, t)] = \ln[K_{\text{aerosol}} \langle C_{\text{aerosol}}(t) \rangle] + \alpha_{\text{aerosol}}(t) \ln(\lambda). \quad (5)$$

By considering, at each time, the four wavelengths in the visible range (0.47, 0.52, 0.59 and 0.66 μm), the application of Eq. (5) to all the hourly aerosol absorption coefficients calculated from the PICO-NARE site available data (July 2001–June 2005) allowed the determination of the $\alpha_{\text{aerosol}}(t)$. Results are summarized in the histogram form, presented in Fig. 2.

For α (BC absorption exponent) value the histogram maximum (-1.0 ± 0.2) was used (this value is consistent with the one proposed by Hansen (2002) for the Aethalometer's "pure" BC), and for β (the dust absorption exponent), the value of the left extreme of the histogram, where the frequency line touches the zero, (-4.0 ± 0.2) was assumed as an

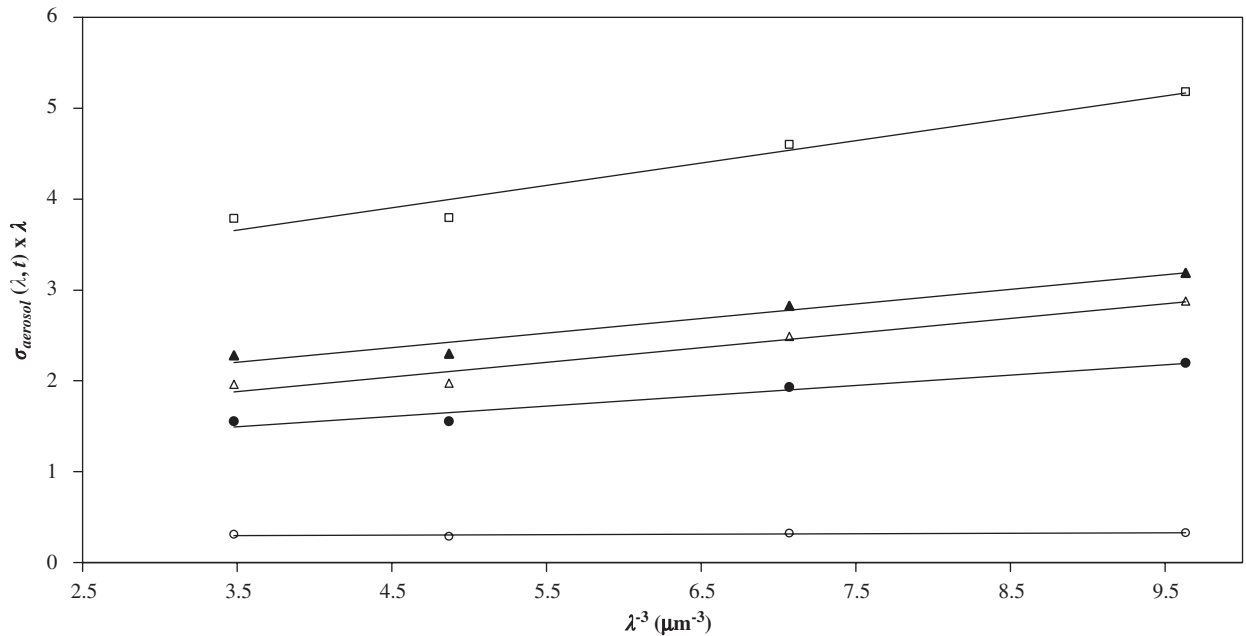


Fig. 3. Symbols represent the experimental results of aerosol absorption coefficients, $\sigma_{\text{aerosol}}(\lambda, t)$, determined for each SPOT (where t is associated to the central time of the SPOT sampling interval), showed in Table 1, represented according to the expected linear behavior proposed by Eq. (6) (SPOT111—solid circle; SPOT112—open square; SPOT113—solid triangle; SPOT114—open triangle; SPOT115—open circle).

approximation of the “pure” dust. This β value is different from the one we previously reported (Fialho et al., 2005). We consider this new value a better estimation, because the histogram reported here (Fig. 2) includes more observations (all the data available from July 2001 through summer 2005 at PICO-NARE site were used) than the one used to estimate the value suggested in the Fialho et al. (2005) paper. (In that paper only the small period of the reported study, 27 July–1, August 2001, was considered). The extreme value of the histogram is the best estimate that we can obtained at this time, and is appropriate because samples with very low values of BC correspond to the larger negative values of β . We must also take in consideration that while the mixing model admits a simple linear combination of the two “pure” contributions (BC and dust aerosol) (Fialho et al.), this is not necessarily true in the real world.

Using these α and β values Eq. (4) can be rewritten,

$$\sigma_{\text{aerosol}}(\lambda, t) \times \lambda = K_{\text{BC}} \langle C_{\text{BC}}(t) \rangle + K_{\text{dust}} \langle C_{\text{dust}}(t) \rangle \lambda^{-3}. \quad (6)$$

Representing the experimental aerosol absorption coefficients associated with the five spots under study (Table 1) according to the linear behavior proposed by Eq. (6) results in the plot shown in Fig. 3. We applied the linear least square regression analysis to the experimental results, considering λ^{-3} as the independent variable and using λ values in the visible range: 0.47, 0.52, 0.59 and 0.66 μm . The dependent variable was $\sigma_{\text{aerosol}}(\lambda, t) \times \lambda$, for each spot. $K_{\text{dust}} \langle C_{\text{dust}}(t) \rangle$ is calculated from each slope and $K_{\text{BC}} \langle C_{\text{BC}}(t) \rangle$ from each intercept; these results are presented in Table 3.

We expect one proportionality relation between the elemental iron concentration, measured with the INAA, and the values $K_{\text{dust}} \langle C_{\text{dust}}(t) \rangle$ taken from the adjustment of Eq. (6) translated by,

$$K_{\text{Fe}} = \frac{K_{\text{dust}} \langle C_{\text{dust}}(t) \rangle}{\langle C_{\text{Fe}}(t) \rangle}. \quad (7)$$

The result of the application of Eq. (7) to each of the SPOT values is presented in the last column of Table 3. The value for SPOT115 is not calculated, as the slope value is statistically zero, resulting in a K_{Fe} value with no statistical significance. The resulting values of K_{Fe} are not significantly different from one another, as expected. The average result of four K_{Fe} values, $0.234 \pm 0.022 \mu\text{m}^4 \text{m}^2 \text{g}^{-1}$, is the best estimation of the calibration constant needed to determined iron concentration using the Aethalometer.

Table 3

Slopes, $K_{\text{dust}} \langle C_{\text{dust}}(t) \rangle$, and intercepts, $K_{\text{BC}} \langle C_{\text{BC}}(t) \rangle$, resulting of applying the least squares method to the model proposed by Eq. (6) for each sample spot interval

Sample	$K_{\text{BC}} \langle C_{\text{BC}}(t) \rangle$	$K_{\text{dust}} \langle C_{\text{dust}}(t) \rangle$ (μm^3)	R	K_{Fe} ($\mu\text{m}^4 \text{m}^2 \text{g}^{-1}$)
SPOT111	1.10 ± 0.24	0.113 ± 0.036	0.976	0.247 ± 0.056
SPOT112	2.80 ± 0.50	0.246 ± 0.076	0.977	0.214 ± 0.037
SPOT113	1.64 ± 0.32	0.160 ± 0.046	0.979	0.212 ± 0.037
SPOT114	1.31 ± 0.32	0.161 ± 0.046	0.980	0.260 ± 0.046
SPOT115	0.281 ± 0.044	0.0049 ± 0.0064	0.730	—

Each value is shown with the respective standard error. Correlation coefficients, R , are presented for each fitting. K_{Fe} values are calculated from application of Eq. (7).

4. Conclusions

Considering now the hourly data for the aerosol absorption coefficients, application of Eq. (6), allows the hourly determination of $K_{\text{dust}} \langle C_{\text{dust}}(t) \rangle$ and $K_{\text{BC}} \langle C_{\text{BC}}(t) \rangle$ (Fialho et al., 2005). The division of $K_{\text{dust}} \langle C_{\text{dust}}(t) \rangle$ by K_{Fe} results in the hourly variability of iron concentration shown in Fig. 4. The calculated values for elemental iron concentration vary from 0.00–1.77 $\mu\text{g}(\text{Fe}) \text{m}^{-3}$, with error variability from 0.02 to 0.38 $\mu\text{g}(\text{Fe}) \text{m}^{-3}$. The total iron mass calculated from these hourly values is $13.2 \pm 1.8 \mu\text{g}(\text{Fe})$ which compares well with the total iron mass calculated from the aerosol absorption coefficients taken from Table 1, $14.0 \pm 1.3 \mu\text{g}(\text{Fe})$, and which also agrees well with the value of $14.84 \pm 0.70 \mu\text{g}$, measured by the INAA technique as was expected.

With the intent to show that BC and dust are not correlated, as would be expected, we applied the manufacture calibration value for black carbon ($K_{\text{BC}} = 14.625 \mu\text{m}^2 \text{g}^{-1}$; Hansen, 2003) to estimate also the hourly and SPOT

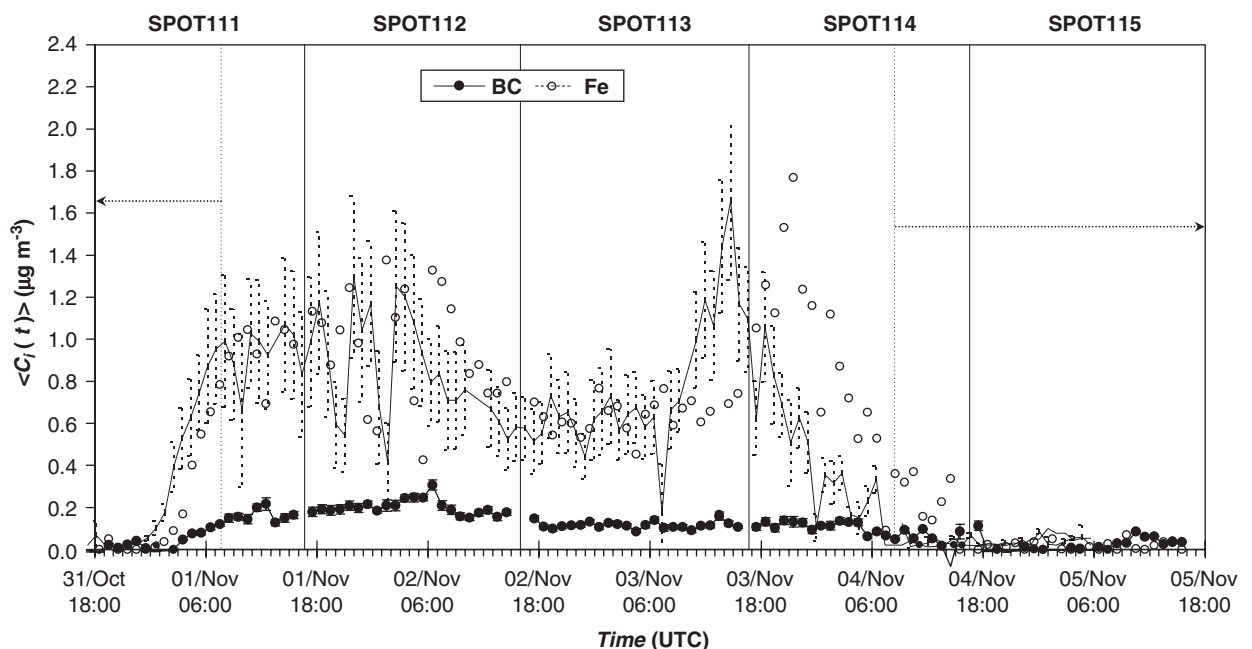


Fig. 4. Solid circles with error bars connected with solid lines, represent the hourly BC concentration variability calculated from the application of Eqs. (6) and (7) to the hourly aerosol absorption coefficients measured with the Aethalometer. Open circles with error bars connected with dashed lines, represent the hourly dust concentration variability calculated from the application of Eqs. (6) and (7) to the hourly aerosol absorption coefficients measured with the Aethalometer. In the left axis legend the i subscript in the average concentration notation, stands for BC or dust.

black carbon concentration during the period in study,

$$\langle C_{\text{BC}}(t) \rangle = \frac{K_{\text{BC}} \langle C_{\text{BC}}(t) \rangle}{14.625}. \quad (8)$$

The black carbon hourly values vary between 0.000 and 0.306 $\mu\text{g m}^{-3}$, with error variability from 0.015 and 0.041 $\mu\text{g m}^{-3}$ (Fig. 4). The total black carbon mass calculated from these hourly values is $2.45 \pm 0.16 \mu\text{g}$, in good agreement with the value of $2.31 \pm 0.12 \mu\text{g}$ obtained for the SPOT aerosol absorption coefficient information.

We have demonstrated the use of multi-wavelength Aethalometer measurements to determine the iron content associated with the iron oxides present in the aerosol dust. We hope that this information can be used to improve the estimation and speciation between the BC and dust aerosol, resulting from optical measurements. For those that have not the resources to make their own calibrations the use of the calibrating constant here presented could be used as an approximation, in the similar way we use the manufacture value ($K_{\text{BC}} = 14.625 \mu\text{m}^2 \text{g}^{-1}$; Hansen, 2003) for the calculation of BC concentration. Whenever possible, the calibration of the Aethalometer should be done and the proper value used. This paper describes one approach for doing this calibration and how to use it to study the iron concentration variability, present on dust aerosol (usually in the form of hematite), with a time resolution (depending on the Aethalometer sampling interval—starts on 5 minutes) not yet reported according to the authors knowledge.

Acknowledgments

We gratefully acknowledge the sponsors of this work: Fundação para a Ciência Tecnologia (FCT - Portugal) Project POCTI-32649-CTA-2000 and grant SFRH/BD/9049/2002; Governo Regional dos Açores (Portugal); Força Aérea Portuguesa (FAP); Bombeiros Voluntários da Madalena do Pico (Portugal); United States National Oceanic and Atmospheric Administration (NOAA) grants NA16GP1658, NA86GP0325 and NA030AP430002; United States National Science Foundation (NSF) grants ATM-0215843 and INT-0110397.

References

- Ackerman, T. P., & Toon, O. B. (1981). Absorption of visible radiation in the atmosphere containing mixtures of absorbing and nonabsorbing particles. *Applied Optics*, 20(20), 3661–3668.
- Alves, L. C., Reis, M. A., & Freitas, M. C. (1998a). Air particulate matter characterization of a rural area in Portugal. *Nuclear Instruments and Methods in Physics Research*, B136/138, 941–947.
- Alves, L. C., Reis, M. A., & Freitas, M. C. (1998b). Elemental analysis of particulate matter and source profile in Lisboa. *X-Ray Spectrometry*, 27, 313–320.
- Arimoto, R., Balsam, W., & Schloesslin, C. (2002). Visible spectroscopy of aerosol particles collected on filters: Iron-oxide minerals. *Atmospheric Environment*, 36, 89–96.
- Baumgardner, D., Raga, G., Peralta, O., Rosas, I., Castro, T., Kuhlbusch, T. et al. (2002). Diagnosing black carbon trends in large urban areas using carbon monoxide measurements. *Journal of Geophysical Research*, 107(D21), 8342.
- Bodhaine, B. A. (1995). Aerosol absorption measurements at Barrow, Mauna Loa and the South Pole. *Journal of Geophysical Research*, 100(D5), 8967–8975.
- Bohren, C. F., & Huffman, D. R. (1998). *Absorption and scattering of light by small particles* (pp. 436–439). New York: WileyInterscience, (Paper Edition).
- Caqueneau, S., Gaudichet, A., Gomes, L., Magonthier, M. C., & Chatenet, B. (1998). Saharan dust: Clay ratio as a relevant tracer to assess the origin of soil-derived aerosols. *Geophysical Research Letters*, 25(7), 983–986.
- Coen, M. C., Weingartner, E., Schaub, D., Hueglin, C., Corrigan, C., Schwilkowski, M. et al. (2003). Saharan dust events at the Jungfraujoch: Detection by wavelength dependence of the single scattering albedo and analysis of the events during the years 2001 and 2002. *Atmospheric Chemistry and Physics Discussions*, 3, 5547–5594.
- De Corte, F. (1987). The k_0 -Standardization method: A move to the optimization of neutron activation analysis. *Habilitation Thesis*, University of Gent.
- Draxler, R. R., & Hess, G. D. (1997). Description of the HYSPLIT_4 modeling system, *NOAA Technical Memorandum ERL ARL-224*, December 24p.
- Draxler, R. R., & Hess, G. D. (1998). An overview of the HYSPLIT_4 modeling system for trajectories, dispersion and deposition. *Australian Meteorological Magazine*, 47, 295–308.
- Draxler, R., & Rolph, G. (2003). HYSPLIT4 (Hybrid Single-Particle Lagrangian Integrated Trajectory) model, Web address: <http://www.arl.noaa.gov/ready/hysplit4.html>, NOAA Air Resources Laboratory, Silver Spring, MA.
- Farinha, M. M., Freitas, M. C., Almeida, S. M., & Reis, M. A. (2001). Some improvements on air particulate matter analysis by INAA. *Radiation Physics and Chemistry*, 61(3-6), 659–661.

- Fialho, P., Hansen, A. D. A., & Honrath, R. E. (2005). Absorption coefficients by aerosols in remote areas: A new approach to decouple dust and black carbon absorption coefficients using seven-wavelength Aethalometer data. *Journal of Aerosol Science*, 36(2), 267–282.
- Freitas, M. C., Almeida, S. M., Reis, M. A., & Oliveira, O. R. (2003). Monitoring trace elements by nuclear techniques in PM10 and PM2.5. *Nuclear Instruments and Methods in Physics Research A*, 505, 430–434.
- Freitas, M. C., & Martinho, E. (1989). Neutron activation analyses of reference materials by the k_0 -standardization and relative method. *Analytica Chimica Acta*, 219, 317–322.
- Gillespie, J. B., & Lindberg, J. D. (1992). Ultraviolet and visible imaginary refractive index of strongly absorbing atmospheric particulate matter. *Applied Optics*, 31(12), 2112–2115.
- Hansen, A. D. A. (2003). *The Aethalometer Manual*. Berkeley, CA, USA: Magee Scientific.
- Honrath, R. E., & Fialho, P. (2002). The Azores Islands: A unique location for ground-based measurements in the MBL and FT of the Central North Atlantic. *IGACActivities Newsletter*, Issue no 24, pp. 20–21.
- Honrath, R. E., Owen, R. C., Val Martin, M., Reid, J. S., Prins, E., Fialho, P. et al. (2004). Regional and hemispheric impacts of anthropogenic and biomass burning emissions on summertime CO and O₃ in the North Atlantic lower free troposphere. *Journal of Geophysical Research*, 109, D24310.
- Hubanks, P. A., Remer, L. A., & Kaufman, Y. J. (MODIS). Images available from the MODIS-Atmosphere web site (<http://modis-atmos.gsfc.nasa.gov>).
- Kleissl, J. (2005). *Personal communication*.
- Kleissl, J., & Honrath, R. (2005). Analysis and application of Sheppard's airflow model to predict mechanical orographic lifting and the occurrence of mountain clouds. *Journal of Applied Meteorology*, submitted for publication.
- Lindberg, J. D., Douglass, R. E., & Garvey, D. M. (1993). Carbon and the optical properties of atmospheric dust. *Applied Optics*, 32(30), 6077–6081.
- Mindat.org, (2005). Mineralogy Database. (<http://www.mindat.org/min-1856.html>).
- Sokolik, I. N., & Toon, O. B. (1999). Incorporation of mineralogical composition into models of the radiative properties of mineral aerosol from UV to IR wavelengths. *Journal of Geophysical Research*, 104(D8), 9423–9444.
- Stunder, B. J. B. (1997). NCEP model output-FNL archive data: TD-6141, Tech. Rep., NOAA—Air Resources Laboratory, Silver Spring, MD 20910, available from (<http://www.arl.noaa.gov/ready-bin/fnl.pl>).
- Tomza, U., Arimoto, R., & Ray, B. J. (2001). Color-related differences in the chemical composition of aerosol-laden filters. *Atmospheric Environment*, 35, 1703–1709.

